

Unconventional superconductivity in systems with annular Fermi surfaces: Application to rhombohedral trilayer graphene

Areg Ghazaryan,^{1,*} Tobias Holder,^{2,*} Maksym Serbyn,¹ and Erez Berg²

¹*IST Austria, Am Campus 1, 3400 Klosterneuburg, Austria*

²*Department of Condensed Matter Physics, Weizmann Institute of Science, Rehovot 76100, Israel*

We show that in a two-dimensional electron gas with an annular Fermi surface, long-range Coulomb interactions can lead to unconventional superconductivity by the Kohn-Luttinger mechanism. Superconductivity is strongly enhanced when the inner and outer Fermi surfaces are close to each other. The most prevalent state has chiral p-wave symmetry, but d-wave and extended s-wave pairing are also possible. We discuss these results in the context of rhombohedral trilayer graphene, where superconductivity was recently discovered in parameter regimes where the normal state has an annular Fermi surface. Using realistic parameters, our mechanism can account for the order of magnitude of T_c in that system, as well as its trends as a function of electron density and perpendicular displacement field. Moreover, it naturally explains some of the outstanding puzzles in this material, that include the weak temperature dependence of the resistivity above T_c , and the proximity of spin singlet superconductivity to the ferromagnetic region in the phase diagram.

Introduction.—Graphene based two-dimensional materials offer a unique platform to study correlated electron phenomena with an unprecedented level of control [1–10]. Among these, rhombohedral trilayer graphene (RTG) [11–14] has recently been shown to exhibit a rich phase diagram, including a plethora of spin and valley polarized states, tunable by varying the electron density and perpendicular electric field [15]. Most strikingly, at least two distinct superconducting phases were discovered in different regions of the phase diagram [16]. The emergence of superconductivity in this ultra-pure and tunable system calls for a theoretical understanding, potentially shedding light on long-standing problems in condensed matter physics and opening the way to future applications.

In this work, we examine the key experimental facts about superconductivity in RTG, and identify two puzzles that seem difficult to reconcile with conventional, phonon-mediated superconductivity. We argue that these puzzles can be resolved if one assumes an unconventional mechanism for superconductivity [17]. Interestingly, superconductivity is found in regimes where the normal-state Fermi surface (FS) has an annular shape, with an inner electron pocket and an outer hole pocket. We show that an annular FS is favorable for an electronic mechanism for superconductivity [18–24], driven by repulsive Coulomb interactions. Using a microscopic model for RTG with realistic parameters, we find that the most likely candidate for the superconducting order parameter is a chiral p-wave, although an extended s-wave [25] is also possible.

Superconductivity in RTG.—The band structure of RTG [11, 12] exhibits strong peaks in the density of states, tunable by a perpendicular electric field, at finite density of electron or holes. As a result, upon doping, RTG undergoes a cascade of phase transitions between different spin and valley polarized phases [15], reminiscent of the observation in twisted bilayer graphene [26, 27]. Note,

however, that in Refs. [15, 16] there is no moiré lattice.

Recently, two superconducting phases were discovered in the hole-doped side, labelled by SC1 and SC2 [16]. SC1 is found within the flavor-symmetric phase. Its maximum critical temperature is $T_{c1} \approx 100$ mK. SC2 occurs within a fully spin-polarized, valley-unpolarized half-metal, and its maximum critical temperature is $T_{c2} \lesssim 50$ mK. In both phases, the coherence length is shorter than the mean free path, placing them in the clean limit. The in-plane critical magnetic field of SC1 is consistent with the Clogston-Chandrasekhar (or Pauli) limit [28, 29], while the in-plane critical field of SC2 exceeds the limit by at least an order of magnitude.

It has been proposed [30] that RTG is a ‘conventional’ phonon-driven superconductor, with a gap function that is nearly uniform (i.e., s-wave like) within each valley. While the nature of superconductivity in RTG is yet to be established, we point out two difficulties with this scenario. First, coupling to acoustic phonon modes should lead to a linear dependence of the resistivity for $T \gtrsim \Theta_{BG}/4$, where Θ_{BG} is the Bloch-Grüneisen temperature, $\Theta_{BG} = 2k_F v_s$ (v_s is the speed of sound). At the density range of SC1, $\Theta_{BG} \approx 40$ K. However, the resistance of RTG above SC1 is nearly temperature-independent up to $T = 20$ K [16]. This is unlike many conventional superconductors, where good agreement is observed between the dimensionless electron-phonon coupling λ estimated from T_c and λ estimated from the slope of the resistivity vs. T [31]. Second, SC1 emerges out of a spin- and valley-unpolarized normal state [15, 16]. As explained below, SC1 can be either spin singlet or triplet, and one expects the inter-valley exchange coupling J_H to determine which one is realized. Experimentally, SC1 is spin singlet, which implies $J_H < 0$ for an s-wave like gap function. This is in apparent contradiction with the presence of a spin polarized ferromagnetic state nearby in the phase diagram, that requires $J_H > 0$ [32].

Below, we argue that both of these puzzles are resolved if one assumes an all-electronic mechanism that leads to unconventional superconductivity.

* A.G. and T.H. have contributed equally to this work.

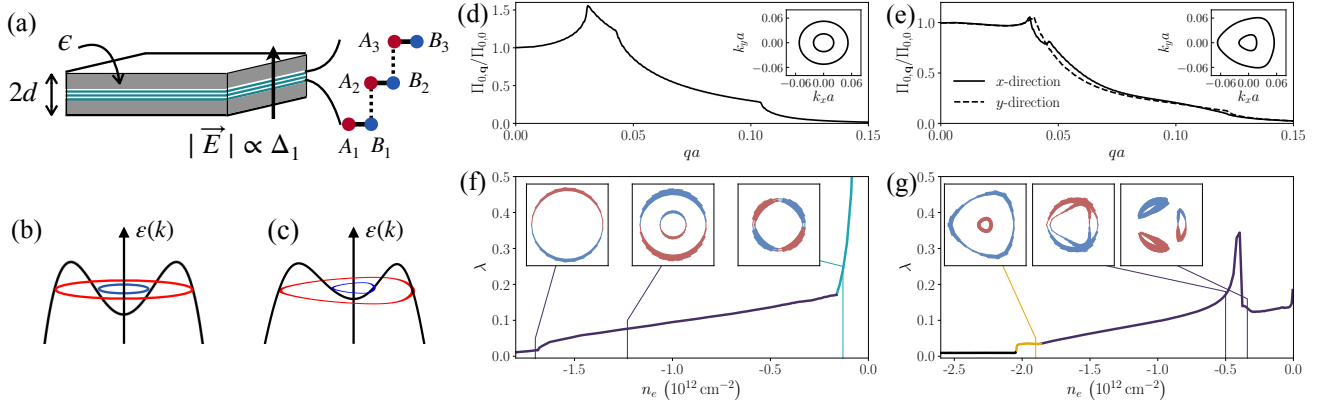


Figure 1. (a) RTG placed between two metallic gates at distance d away, and encapsulated by an insulator with dielectric constant ϵ . (b,c) Band structure and FS of the simplified circularly symmetric model and the realistic model, respectively. (d,e) The polarization function $\Pi_{0,\mathbf{q}}$ within the simplified and realistic models, at density $n_e = -1.19 \times 10^{12} \text{ cm}^{-2}$ and $n_e = -1.67 \times 10^{12} \text{ cm}^{-2}$, respectively. (f,g) SC dimensionless coupling constant, λ , vs. density in the two models, colored for p-wave (purple), extended s-wave (yellow) and d-wave (cyan). The inset shows the solution of the linearized gap equation along the FS at certain values of n_e . Red and blue represent positive and negative $\Delta_{\mathbf{k}}$, respectively. Panels (f-g) were obtained with $\epsilon = 4$ and $d = 36.9 \text{ nm}$. In (e,g) we used $\Delta_1 = 20 \text{ meV}$.

Model.—The unit cell structure of rhombohedral trilayer graphene is shown schematically in Fig. 1(a). We write the Hamiltonian as

$$\hat{H} = \hat{H}_0 + \hat{H}_C, \quad (1)$$

where $\hat{H}_0 = \sum_{\mathbf{k},\tau,s} \Psi_{\mathbf{k}\tau s}^\dagger h_{\mathbf{k}\tau} \Psi_{\mathbf{k}\tau s}$ is the single-particle part [12]. $h_{\mathbf{k}\tau}$ is a 6×6 matrix in the basis $(A_1, B_1, A_2, B_2, A_3, B_3)$, corresponding to the A, B sublattices of layers 1,2,3 (Fig. 1(a)) that is written explicitly in the Supplemental Material [33]. The valley and spin indices are denoted by τ and s , respectively. $\Psi_{\mathbf{k}\tau s}^\dagger$ is a spinor containing the operators $\psi_{\mathbf{k},\ell,\sigma,\tau,s}^\dagger$, that create an electron with momentum \mathbf{k} , at layer $\ell = 1, 2, 3$ and sublattice $\sigma = A, B$. The Coulomb interaction is given by

$$\hat{H}_C = \frac{1}{2L^2} \sum_{\mathbf{q}} V_{0,\mathbf{q}} \rho_{\mathbf{q}} \rho_{-\mathbf{q}}, \quad (2)$$

where $V_{0,\mathbf{q}} = \frac{2\pi e^2}{\epsilon q} \tanh(qd)$ is the Coulomb potential screened by two metallic gates at distance d above and below the RTG, ϵ is the effective dielectric constant, and L is the linear dimension of the system. The Fourier component of the density is given by $\rho_{\mathbf{q}} = \sum_{\mathbf{k}\tau s} \Psi_{\mathbf{k}\tau s}^\dagger \Psi_{\mathbf{k}+\mathbf{q}\tau s}$.

Near the Fermi level, the band structure of $h_{\mathbf{k}\tau}$ consists of a conduction and a valence band separated by a gap, $2\Delta_1$, proportional to the perpendicular displacement field. The other four bands are split by at least 200 meV. Δ_1 and the carrier density, n_e , controlled experimentally by gate voltages, can be used to tune the system between different phases.

We project the Hamiltonian onto the valence band, where SC1 and SC2 occur. This amounts to substituting $\rho_{\mathbf{q}}$ by $\tilde{\rho}_{\mathbf{q}} = \sum_{\mathbf{k},\tau,s} \Lambda_{\mathbf{k},\mathbf{q},\tau} c_{\mathbf{k},\tau,s}^\dagger c_{\mathbf{k}+\mathbf{q},\tau,s}$, where $c_{\mathbf{k},\tau,s}^\dagger$ creates an electron at momentum \mathbf{k} in the valence band in valley

τ and spin s , and $\Lambda_{\mathbf{k},\mathbf{q},\tau} = \langle u_{\mathbf{k},\tau} | u_{\mathbf{k}+\mathbf{q},\tau} \rangle$ is an overlap between Bloch wave functions of the valence band, $|u_{\mathbf{k},\tau}\rangle$.

We investigate superconductivity within a purely electronic mechanism, driven by the Coulomb interaction. Within this mechanism [18, 20], pairing is mediated by particle-hole electronic fluctuations at a broad range of energies. The effective interaction after screening by such fluctuations depends on frequency only weakly, and will be treated as instantaneous. Within the random phase approximation (RPA), this interaction is given by

$$V_{\mathbf{q}} = \frac{V_{0,\mathbf{q}}}{1 + \Pi_{0,\mathbf{q}} V_{0,\mathbf{q}}}, \quad (3)$$

where $\Pi_{0,\mathbf{q}} = N \sum_{\mathbf{k}} |\Lambda_{\mathbf{k},\mathbf{q},\tau}|^2 \frac{f(\epsilon_{\mathbf{k},\tau}) - f(\epsilon_{\mathbf{k}+\mathbf{q},\tau})}{\epsilon_{\mathbf{k}+\mathbf{q},\tau} - \epsilon_{\mathbf{k},\tau}}$ is the static polarization function, with $\epsilon_{\mathbf{k},\tau}$ being the dispersion of the valence band in valley τ . $f(\epsilon)$ is the Fermi function. $N = 4$ is the number of spin and valley flavors. Note that $\Pi_{0,\mathbf{q}}$ is independent of τ , due to time reversal symmetry.

The RPA interaction Hamiltonian is given by $\hat{H}_{\text{RPA}} = \frac{1}{2L^2} \sum_{\mathbf{q}} V_{\mathbf{q}} \tilde{\rho}_{\mathbf{q}} \tilde{\rho}_{-\mathbf{q}}$. The superconducting T_c is found by solving the linearized Bardeen-Cooper-Schrieffer (BCS) gap equation using Eq. (3) as the pairing interaction. For a formal justification of this procedure, as well as a derivation of the linearized gap equation, see [33]. The gap equation is given by

$$\Delta_{\mathbf{k}} = -\log\left(\frac{W}{T_c}\right) \int_{\text{FS}} \frac{dk'_{\parallel}}{(2\pi)^2 v_{\mathbf{k}'}} V_{\mathbf{k}-\mathbf{k}'} |\Lambda_{\mathbf{k},\mathbf{k}'-\mathbf{k},+1}|^2 \Delta_{\mathbf{k}'}, \quad (4)$$

where $\Delta_{\mathbf{k}}$ is the SC order parameter at a point \mathbf{k} on the FS in valley $\tau = +1$, $v_{\mathbf{k}}$ is the magnitude of the Fermi velocity at that point, and W is an upper cutoff of the order of the Fermi energy. The integration is taken over all the FSs. Denoting λ as the largest eigenvalue of the linear operator

\mathcal{M} defined by $\mathcal{M}\Delta_{\mathbf{k}} = -\int \frac{dk'_\parallel}{(2\pi)^2 v_{\mathbf{k}'}} V_{\mathbf{k}-\mathbf{k}'} |\Lambda_{\mathbf{k},\mathbf{k}'-\mathbf{k},+1}|^2 \Delta_{\mathbf{k}'}$, we obtain $T_c = W e^{-1/\lambda}$. Our goal is to calculate λ .

Kohn-Luttinger mechanism: idealized model.—As is well known, since $V_{\mathbf{q}} > 0$ for all \mathbf{q} , a solution for Eq. (4) must have a $\Delta_{\mathbf{k}}$ that changes sign across the FS. Therefore, the solution typically has a non s-wave symmetry, depending on the structure of $\Pi_{0,\mathbf{q}}$. For a single parabolic band in two dimensions, $\Pi_{0,\mathbf{q}}$ is constant up to $q = 2k_F$, and Eq. (4) has no solution [34]. In the case of two subbands with different Fermi momenta, the total polarization function is no longer a constant for momenta smaller than $2k_F$ of the outer FS, and non-trivial solutions are obtained [23, 24]. In RTG, both SC1 and SC2 occur in regions where the normal state exhibits an annular FS, where the inner and outer Fermi surfaces have opposite Fermi velocities. Such a dispersion is favorable for superconductivity, as we shall now illustrate.

We begin with a simplified model where the dispersion is approximated as $\varepsilon_{\mathbf{k}} = -\varepsilon_0(k^2/k_0^2 - 1)^2 - \mu$, characterized by an overall energy scale ε_0 and a momentum scale k_0 , chosen to roughly match the dispersion of the valence band. The dispersion is shown in Fig. 1(b). μ is chosen in the regime where the FS consists of two concentric rings. Moreover, we ignore the effects of the wave functions, setting $\Lambda_{\mathbf{k},\mathbf{q},\tau} = 1$.

Due to the rotational symmetry of this model, Eq. (4) can be simplified by transforming to the angular momentum basis. Moreover, $\Pi_{0,\mathbf{q}}$ can be computed analytically [33]. $\Pi_{0,\mathbf{q}}$ is shown for a representative electron density in Fig. 1(d). It exhibits singularities at the characteristic momenta $2k_{F1}$, $2k_{F2}$, and $k_{F1} - k_{F2}$, where $k_{F1,2} = k_0 \sqrt{1 \pm \sqrt{-\mu/\varepsilon_0}}$ are the momenta of the outer and inner FS, respectively.

The result for λ as a function of electron density is shown in Fig. 1(f). At large hole densities where the inner pocket disappears, λ is nearly zero. λ increases discontinuously once the inner pocket appears (around $n_e = -1.7 \cdot 10^{12} \text{ cm}^{-2}$). The dominant superconducting instability in this regime has p-wave symmetry. Upon decreasing the density of holes, λ increases gradually. Approaching the zero hole density limit, λ increases sharply, and the dominant pairing channel changes to d-wave. λ diverges in the limit $n_e \rightarrow 0$, due to the diverging density of states [33].

Kohn-Luttinger mechanism in RTG.—Turning to RTG, we use a realistic model for the band structure and $\Lambda_{\mathbf{k},\mathbf{q},\tau}$ [33]. The resulting FS and polarization function $\Pi_{0,\mathbf{q}}$ are shown for a representative density in Fig. 1(e). The FSs of the inner and outer pockets show a substantial trigonal warping. Correspondingly, $\Pi_{0,\mathbf{q}}$ is anisotropic. However, some of the features are similar to those of the circularly symmetric model. λ as a function of density (Fig. 1(g)) is qualitatively similar to that of the circularly symmetric model, showing a sharp increase at the density where the inner pocket appears ($n_e \approx -2.1 \cdot 10^{12} \text{ cm}^{-2}$), followed by a gradual increase of λ with decreasing hole density. The symmetry of the order parameter changes from

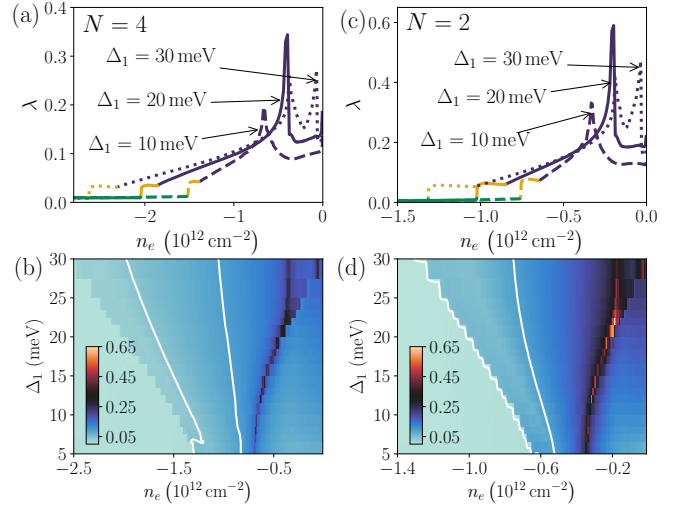


Figure 2. (a,b) Coupling constant λ as a function of density and displacement field Δ_1 for the unpolarized state, $N = 4$. (c,d) Same as a,b assuming the spin polarization, $N = 2$. The color coding in (a,c) is identical to Fig. 1. The white contours in (b,d) indicate $\lambda = 0.05, 0.1$.

extended s-wave (symmetry representation A_1 according to the point group C_{3v} of RTG with a perpendicular electric field), with an opposite sign on the inner and outer Fermi pockets, to p-wave (representation E). Note that within the symmetry of RTG, p-wave and d-wave are not distinct from each other. λ diverges logarithmically at the Van Hove density $n_e \approx -0.5 \cdot 10^{12} \text{ cm}^{-2}$, where the annulus reconstructs into three disconnected pockets.

Focusing on the p-wave phase and going beyond the linearized gap equation, the favored state below T_c is a chiral $p_x + ip_y$ state. This result is derived the SM [33] by considering the quartic terms in the Ginzburg-Landau free energy functional.

Importantly, within our model, Eq (1), spin singlet and triplet pairing are degenerate, independently of the orbital symmetry of the order parameter. This counter-intuitive result follows from the $SU(2) \times SU(2)$ symmetry of the Hamiltonian, which allows to rotate the spin of one valley relative to the other [30, 35, 36]. In the singlet (triplet) case, the order parameter in valley $\tau = +1$ has the same (opposite) phase to that of valley -1 , respectively, such that the Pauli principle is obeyed. We shall discuss the lifting of the singlet-triplet degeneracy below.

Fig. 2(a,b) shows the density and Δ_1 dependence of λ in the spin and valley unpolarized phase [$N = 4$ in Eq. (3)], corresponding to SC1 region in experiment [16]. Increasing Δ_1 shifts the sharp peak corresponding to the Van Hove singularity towards charge neutrality. However, there is a broad density regime ($n_e < -0.8 \cdot 10^{12} \text{ cm}^{-2}$) where λ is an increasing function of Δ_1 at a fixed density, following the trend of the density of states with Δ_1 in this regime. This is consistent with the fact that the SC1 phase is entered upon increasing electric field in the unpolarized phase [16]. To account for $T_c = 0.1 \text{ K}$ in SC1, assuming

that $W \approx E_F \approx 50$ K, we need $\lambda \approx 0.16$. As seen in Fig. 2, our theory is capable of producing values of λ of this order. In the vicinity of the Van Hove points, λ diverges logarithmically, and our theory breaks down. The Van Hove points are not attained in experiment, since they are preceded by Stoner transitions due to high density of states [15]. We note that the dispersion features a higher order Van Hove singularity at $\Delta_1 \approx 18$ meV [33, 37].

Fig. 2(c,d) shows λ as a function of density and Δ_1 assuming a spin polarized, valley-unpolarized state ($N = 2$), corresponding to SC2. The overall trends are similar to the spin unpolarized phase, although for $N = 2$, the pairing is necessarily spin triplet. The magnitude of λ is somewhat larger than for $N = 4$, since the effective interaction [Eq. (3)] is stronger for $N = 2$. This is in apparent disagreement with experiment. We speculate that the reason for this discrepancy is the residual Hund's coupling, not considered in Eq. (1), which may favor spin singlet pairing (see below).

Finally, in Fig. 3 we show the dependence of λ on the dielectric constant ϵ and the distance to the gates, d , for three values of the electron density. λ increases with decreasing ϵ , as can be expected from the fact that within our mechanism, superconductivity originates directly from repulsive interactions. Interestingly, λ is nearly independent of d for $d \gtrsim 4$ nm. This is since the pairing comes primarily from large momentum scattering processes where q is of the order of $2k_F$, k_F being the Fermi momentum within a valley [38]. As long as the gate is sufficiently far such that $2k_F \gtrsim 1/d$, the effective interaction strength at $q \lesssim 2k_F$ is nearly independent of d .

Role of the Hund's coupling.—We now discuss the lifting of the degeneracy between singlet and triplet pairing. This requires an inter-valley interaction that depend on the relative spin of the two electrons. Such an interaction is expected to be short-ranged in real space, and receives contributions from the short-range part of the Coulomb interaction and from electron-phonon coupling [39, 40]. The simplest term of this form is an inter-valley Hund's coupling, of the form

$H_{\text{Hund}} = -J_H \int d^2r \mathbf{S}_+ \cdot \mathbf{S}_-$, where \mathbf{S}_{\pm} are the spin densities in the two valleys, and J_H may be of either sign.

In general, $J_H > 0$ ($J_H < 0$) favors triplet (singlet) pairing, respectively. However, considering e.g. a $p_x + ip_y$ state, one can easily verify that H_{Hund} drops out of the linearized gap equation (4). Hence, this term does not lift the singlet-triplet degeneracy [33]. Physically, this is because H_{Hund} is local in real space, and since the $p_x + ip_y$ state has a non-zero angular momentum, the amplitude of the two electrons to be at the same location vanishes.

To lift the degeneracy in the $p_x + ip_y$ state, one needs to go beyond the assumption of a momentum independent (i.e., local) Hund's term. To illustrate this, we assume that the effective Hund's coupling depends on distance, $J_H(\mathbf{r} - \mathbf{r}')$. Expanding its Fourier transform \tilde{J}_H at small momenta as: $\tilde{J}_H(\mathbf{q}) = J_{H,0} + J_{H,2}(qa)^2 + O(q^4)$ (where a is the graphene lattice spacing), we find that $J_{H,2} > 0$ ($J_{H,2} < 0$) favors singlet (triplet) pairing [33]. Hence, the lifting of the degeneracy is determined by the sign of the residual non-local Hund's coupling, which can be of either sign relative to $J_{H,0}$, depending on microscopic details. $J_{H,2} > 0$ corresponds to a negative second moment of $J_H(\mathbf{r})$, i.e., the effective Hund's coupling is *antiferromagnetic* in some range of distances, which promotes singlet pairing.

Deriving the effective Hund's term microscopically is notoriously difficult [40]. Instead, we can determine the signs of $J_{H,0}$ and $J_{H,2}$ from the experiment. We assume that $J_{H,0} > 0$, favoring ferromagnetism, and $J_{H,2} > 0$, favoring singlet pairing in the $p_x + ip_y$ phase. Hence, the SC1 phase, which emerges out of a spin-unpolarized normal state, is spin singlet. Note that for a simple s-wave order parameter (with no sign change of $\Delta_{\mathbf{k}}$ within a single valley), the leading-order $J_{H,0}$ term is sufficient to lift the singlet-triplet degeneracy. Hence, $J_{H,0} > 0$ (required by the presence of valley-unpolarized ferromagnets) implies that SC1 – if it were simple s-wave – should be spin triplet, in contradiction with experiment. The normal state of SC2 is a fully spin polarized ferromagnet, and hence it must be spin triplet, although that state is disfavored by $J_{H,2} > 0$. This is consistent with the strong violation of the Pauli limit in SC2, and can at least partially explain the fact that T_c of SC2 is substantially lower than that of SC1 [16]. Finally, we comment that in the extended s-wave state, $J_{H,0}$ does not drop out of the gap equation. However, its effect is still very weak, since the Coulomb repulsion strongly suppresses the amplitude for the two electrons forming a Cooper pair to be close to each other [33].

Discussion.—We have shown that repulsive interactions can give rise to robust unconventional superconductivity in two-dimensional systems with annular FSs. Intriguingly, precisely such FSs are found in RTG in the parameter regimes where superconductivity was recently discovered. The Kohn–Luttinger mechanism is consistent with the absence of a strong temperature dependence of the resistivity above T_c , since it relies on electron-electron interactions that do not contribute to the resistivity in the absence of umklapp scattering. An unconventional SC state can fur-

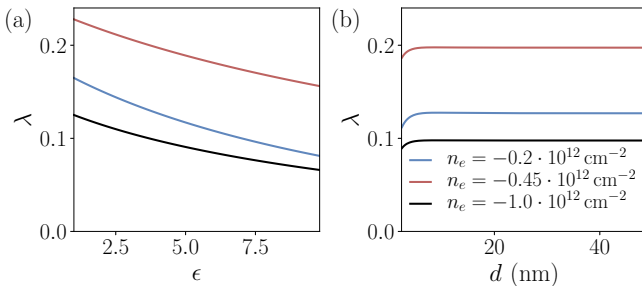


Figure 3. Coupling constant λ as a function of dielectric constant ϵ (a) and distance to the gate d (b). The results are for $\Delta_1 = 20$ meV and densities listed in the legend correspond to the three pocket FS (blue), two annular FS near Van Hove singularity (red) and the regime of annulus away from the singularity (black).

ther explain the apparent discrepancy between SC1 being spin singlet and the presence of a nearby spin polarized phase, implying that the inter-valley exchange coupling is ferromagnetic.

An important outstanding question is, of course, whether the superconducting state in RTG is indeed unconventional. As is well known, such a state would be very sensitive to non-magnetic disorder, and would be destroyed if the elastic mean free path became of the order of the coherence length of the clean system [41–44]. A conventional s-wave SC should be more resilient [45, 46]. Thus, introducing controlled amounts of disorder to the system could be used to identify the nature of the superconducting state. Such a strategy has been applied successfully to other ultra-clean unconventional superconductors [47].

Another prediction of our theory is the near-degeneracy between singlet and triplet pairing. Such a near-degeneracy is expected also within an electron-phonon mechanism, as pointed out in Ref. [30]. As SC1 is suppressed by an in-plane field, a triplet state may be stabilized at lower temperature. So far, T_c of SC1 was found to be suppressed below 50mK with the application of an in-plane field [16], but a triplet SC with a lower T_c is possible. Furthermore, SC2 is a fully spin polarized state, and is expected to have exotic properties, due to the intertwining of the SC phase with the orientation of the magnetization [48].

The most likely pairing state within our theory is a chiral $p_x + ip_y$ SC that breaks time reversal symmetry. This state is expected to generate spontaneous edge currents [49–51]. The symmetry of the order parameter can also be revealed in Josephson interferometry experiments.

The pairing mechanism proposed in this work is mediated by electronic fluctuations with a broad spectrum,

and does not assume the existence of a soft collective mode at low energies (that arises if the system is close to a continuous phase transition). If such soft mode exists, it could enhance T_c further. The possibility of pairing mediated by a soft collective mode in RTG was studied very recently [52, 53], and found to lead to a chiral p-wave state similar to the one discussed here.

Looking forward, it is interesting to ask how to raise T_c in RTG and other systems with annular FSs. Our theory predicts a significant enhancement of λ near the Van Hove singularity where the inner and outer FSs meet. In RTG, the metallic state seems to become unstable towards spin or valley polarization before this point is reached. We speculate that placing the metallic gates closer to the system may suppress these instabilities, while not affecting superconductivity significantly. Our theory predicts that T_c is nearly independent of the distance to the gates down to $d \approx 4\text{nm}$ (Fig. 3), offering a possible route towards increasing T_c in this system.

ACKNOWLEDGMENTS

We thank Yang-Zhi Chou, Andrey Chubukov, Johannes Hofmann, Steve Kivelson, Sri Raghu, and Sankar das Sarma, Jay Sau, Fengcheng Wu, and Andrea Young for many stimulating discussions and for their comments on the manuscript. E.B. thanks S. Chatterjee, T. Wang, and M. Zaletel for a collaboration on a related topic. A.G. acknowledges support by the European Unions Horizon 2020 research and innovation program under the Marie Skłodowska-Curie Grant Agreement No. 754411. E.B. and T.H. were supported by the European Research Council (ERC) under grant HQMAT (Grant Agreement No. 817799), by the Israel-USA Binational Science Foundation (BSF), and by a Research grant from Irving and Cherna Moskowitz.

-
- [1] Benjamin E Feldman, Jens Martin, and Amir Yacoby, “Broken-symmetry states and divergent resistance in suspended bilayer graphene,” *Nature Physics* **5**, 889–893 (2009).
 - [2] AS Mayorov, DC Elias, Marcin Mucha-Kruczynski, RV Gorbachev, T Tudorovskiy, A Zhukov, SV Morozov, MI Katsnelson, VI Fal’ko, AK Geim, *et al.*, “Interaction-driven spectrum reconstruction in bilayer graphene,” *Science* **333**, 860–863 (2011).
 - [3] Yuan Cao, Valla Fatemi, Ahmet Demir, Shiang Fang, Spencer L Tomarken, Jason Y Luo, Javier D Sanchez-Yamagishi, Kenji Watanabe, Takashi Taniguchi, Efthimios Kaxiras, *et al.*, “Correlated insulator behaviour at half-filling in magic-angle graphene superlattices,” *Nature* **556**, 80 (2018).
 - [4] Yuan Cao, Valla Fatemi, Shiang Fang, Kenji Watanabe, Takashi Taniguchi, Efthimios Kaxiras, and Pablo Jarillo-Herrero, “Unconventional superconductivity in magic-angle graphene superlattices,” *Nature* **556**, 43–50 (2018).
 - [5] Xiaobo Lu, Petr Stepanov, Wei Yang, Ming Xie, Mohammed Ali Aamir, Ipsita Das, Carles Urgell, Kenji Watanabe, Takashi Taniguchi, Guangyu Zhang, *et al.*, “Superconductors, orbital magnets and correlated states in magic-angle bilayer graphene,” *Nature* **574**, 653–657 (2019).
 - [6] Xiaomeng Liu, Zeyu Hao, Eslam Khalaf, Jong Yeon Lee, Yuval Ronen, Hyobin Yoo, Danial Haei Najafabadi, Kenji Watanabe, Takashi Taniguchi, Ashvin Vishwanath, *et al.*, “Tunable spin-polarized correlated states in twisted double bilayer graphene,” *Nature* **583**, 221–225 (2020).
 - [7] Matthew Yankowitz, Shaowen Chen, Hryhorii Polshyn, Yuxuan Zhang, K. Watanabe, T. Taniguchi, David Graf, Andrea F. Young, and Cory R. Dean, “Tuning superconductivity in twisted bilayer graphene,” *Science* **363**, 1059–1064 (2019).
 - [8] Guorui Chen, Aaron L Sharpe, Patrick Gallagher, Ilan T Rosen, Eli J Fox, Lili Jiang, Bosai Lyu, Hongyuan Li, Kenji Watanabe, Takashi Taniguchi, *et al.*, “Signatures

- of tunable superconductivity in a trilayer graphene moiré superlattice,” *Nature* **572**, 215–219 (2019).
- [9] Zeyu Hao, AM Zimmerman, Patrick Ledwith, Eslam Khalaf, Danial Haie Najafabadi, Kenji Watanabe, Takashi Taniguchi, Ashvin Vishwanath, and Philip Kim, “Electric field-tunable superconductivity in alternating-twist magic-angle trilayer graphene,” *Science* **371**, 1133–1138 (2021).
 - [10] Jeong Min Park, Yuan Cao, Kenji Watanabe, Takashi Taniguchi, and Pablo Jarillo-Herrero, “Tunable strongly coupled superconductivity in magic-angle twisted trilayer graphene,” *Nature* **590**, 249–255 (2021).
 - [11] Mikito Koshino and Edward McCann, “Trigonal warping and berry’s phase $n\pi$ in ABC-stacked multilayer graphene,” *Phys. Rev. B* **80**, 165409 (2009).
 - [12] Fan Zhang, Bhagawan Sahu, Hongki Min, and A. H. MacDonald, “Band structure of ABC-stacked graphene trilayers,” *Phys. Rev. B* **82**, 035409 (2010).
 - [13] Mikito Koshino, “Interlayer screening effect in graphene multilayers with ABA and ABC stacking,” *Phys. Rev. B* **81**, 125304 (2010).
 - [14] Kin Fai Mak, Jie Shan, and Tony F. Heinz, “Electronic structure of few-layer graphene: Experimental demonstration of strong dependence on stacking sequence,” *Phys. Rev. Lett.* **104**, 176404 (2010).
 - [15] Haoxin Zhou, Tian Xie, Areg Ghazaryan, Tobias Holder, James R. Ehrets, Eric M. Spanton, Takashi Taniguchi, Kenji Watanabe, Erez Berg, Maksym Serbyn, and Andrea F. Young, “Half and quarter metals in rhombohedral trilayer graphene,” arXiv e-prints , arXiv:2104.00653 (2021), arXiv:2104.00653 [cond-mat.mes-hall].
 - [16] Haoxin Zhou, Tian Xie, Takashi Taniguchi, Kenji Watanabe, and Andrea F. Young, “Superconductivity in rhombohedral trilayer graphene,” arXiv e-prints , arXiv:2106.07640 (2021), arXiv:2106.07640 [cond-mat.mes-hall].
 - [17] For a related mechanism for unconventional superconductivity in trilayer graphene, starting from the Hubbard model, see H. Dai, J. Hou, X. Zhang, Y. Liang, and T. Ma, *Phys. Rev. B* **104**, 035104 (2021).
 - [18] W. Kohn and J. M. Luttinger, “New mechanism for superconductivity,” *Phys. Rev. Lett.* **15**, 524–526 (1965).
 - [19] M Yu Kagan, Vitalii A Mitskan, and Maksim Mikhailovich Korovushkin, “Anomalous superconductivity and superfluidity in repulsive fermion systems,” *Physics-Uspekhi* **58**, 733 (2015).
 - [20] S. Raghu, S. A. Kivelson, and D. J. Scalapino, “Superconductivity in the repulsive Hubbard model: An asymptotically exact weak-coupling solution,” *Phys. Rev. B* **81**, 224505 (2010).
 - [21] Saurabh Maiti and Andrey V Chubukov, “Superconductivity from repulsive interaction,” in *AIP Conference Proceedings*, Vol. 1550 (American Institute of Physics, 2013) pp. 3–73.
 - [22] Similarly, a two-dimensional band structure with multiple sub-bands has been predicted to be favorable for an unconventional mechanism for superconductivity [23, 24].
 - [23] S. Raghu and S. A. Kivelson, “Superconductivity from repulsive interactions in the two-dimensional electron gas,” *Phys. Rev. B* **83**, 094518 (2011).
 - [24] Andrey V. Chubukov and Steven A. Kivelson, “Superconductivity in engineered two-dimensional electron gases,” *Phys. Rev. B* **96**, 174514 (2017).
 - [25] I. I. Mazin, D. J. Singh, M. D. Johannes, and M. H. Du, “Unconventional Superconductivity with a Sign Reversal in the Order Parameter of $\text{LaFeAsO}_{1-x}\text{F}_x$,” *Phys. Rev. Lett.* **101**, 057003 (2008).
 - [26] U. Zondiner, A. Rozen, D. Rodan-Legrain, Y. Cao, R. Queiroz, T. Taniguchi, K. Watanabe, Y. Oreg, F. von Oppen, Ady Stern, E. Berg, P. Jarillo-Herrero, and S. Ilani, “Cascade of phase transitions and Dirac revivals in magic-angle graphene,” *Nature (London)* **582**, 203–208 (2020).
 - [27] Dillon Wong, Kevin P Nuckolls, Myungchul Oh, Biao Lian, Yonglong Xie, Sangjun Jeon, Kenji Watanabe, Takashi Taniguchi, B Andrei Bernevig, and Ali Yazdani, “Cascade of electronic transitions in magic-angle twisted bilayer graphene,” *Nature* **582**, 198–202 (2020).
 - [28] A. M. Clogston, “Upper limit for the critical field in hard superconductors,” *Phys. Rev. Lett.* **9**, 266–267 (1962).
 - [29] B. S. Chandrasekhar, “A note on the maximum critical field of high-field superconductors,” *Applied Physics Letters* **1**, 7–8 (1962).
 - [30] Yang-Zhi Chou, Fengcheng Wu, Jay D. Sau, and Sankar Das Sarma, “Acoustic-phonon-mediated superconductivity in rhombohedral trilayer graphene,” arXiv e-prints , arXiv:2106.13231 (2021), arXiv:2106.13231 [cond-mat.supr-con].
 - [31] Philip B Allen, “The electron-phonon coupling constant,” *Handbook of Superconductivity*, edited by Charles P. Poole Jr. (Academic Press, San Diego) **9G**, 478 (2000).
 - [32] A possible resolution is that that J_H changes its sign as a function of density. However, since J_H is a lattice-scale interaction, it seems unlikely to changes significantly upon a small change in electron concentration.
 - [33] See Supplemental Material for more details on the band structure and polarization function of RTG and the circularly symmetric model, the method for calculation of T_c , the SC state below T_c , and the Hund’s coupling.
 - [34] Andrey V. Chubukov, “Kohn-Luttinger effect and the instability of a two-dimensional repulsive Fermi liquid at $T = 0$,” *Phys. Rev. B* **48**, 1097–1104 (1993).
 - [35] Jong Yeon Lee, Eslam Khalaf, Shang Liu, Xiaomeng Liu, Zeyu Hao, Philip Kim, and Ashvin Vishwanath, “Theory of correlated insulating behaviour and spin-triplet superconductivity in twisted double bilayer graphene,” *Nature communications* **10**, 1–10 (2019).
 - [36] Eslam Khalaf, Patrick Ledwith, and Ashvin Vishwanath, “Symmetry constraints on superconductivity in twisted bilayer graphene: Fractional vortices, $4e$ condensates or non-unitary pairing,” arXiv e-prints , arXiv:2012.05915 (2020), arXiv:2012.05915 [cond-mat.supr-con].
 - [37] Noah F. Q. Yuan, Hiroki Isobe, and Liang Fu, “Magic of high-order van Hove singularity,” *Nat. Commun.* **10**, 5769 (2019), arXiv:1901.05432 [cond-mat.str-el].
 - [38] In the case where the FS is composed of disjoint pockets, $2k_F$ should be replaced by the maximum distance between points on the FS.
 - [39] Jason Alicea and Matthew P. A. Fisher, “Graphene integer quantum Hall effect in the ferromagnetic and paramagnetic regimes,” *Phys. Rev. B* **74**, 075422 (2006).
 - [40] Maxim Kharitonov, “Phase diagram for the $\nu = 0$ quantum Hall state in monolayer graphene,” *Phys. Rev. B* **85**, 155439 (2012).
 - [41] A. A. Abrikosov and L. P. Gor’kov, Contribution to the theory of superconducting alloys with paramagnetic impurities, *Zh. Eksp. Teor. Fiz.* **39**, 1781 (1960) [*Sov. Phys. JETP* **12**, 1243 (1961)].

- [42] P. I. Larkin, Vector pairing in superconductors of small dimensions, *Zh. Eksp. Teor. Fiz. Pis'ma Red.* **2**, 205 (1965) [*Sov. Phys. JETP Lett.* **2**, 130 (1965)].
- [43] A. J. Millis, Subir Sachdev, and C. M. Varma, "Inelastic scattering and pair breaking in anisotropic and isotropic superconductors," *Phys. Rev. B* **37**, 4975–4986 (1988).
- [44] R. J. Radtke, K. Levin, H.-B. Schüttler, and M. R. Norman, "Predictions for impurity-induced T_c suppression in the high-temperature superconductors," *Phys. Rev. B* **48**, 653–656 (1993).
- [45] Philip W Anderson, "Theory of dirty superconductors," *Journal of Physics and Chemistry of Solids* **11**, 26–30 (1959).
- [46] A. M. Finkel'stein, "Suppression of superconductivity in homogeneously disordered systems," *Physica B: Condensed Matter* **197**, 636–648 (1994).
- [47] A. P. Mackenzie, R. K. W. Haselwimmer, A. W. Tyler, G. G. Lonzarich, Y. Mori, S. Nishizaki, and Y. Maeno, "Extremely Strong Dependence of Superconductivity on Disorder in Sr_2RuO_4 ," *Phys. Rev. Lett.* **80**, 161–164 (1998).
- [48] Eyal Cornfeld, Mark S. Rudner, and Erez Berg, "Spin-polarized superconductivity: Order parameter topology, current dissipation, and multiple-period Josephson effect," *Phys. Rev. Research* **3**, 013051 (2021).
- [49] Akira Furusaki, Masashige Matsumoto, and Manfred Sigrist, "Spontaneous hall effect in a chiral p-wave superconductor," *Phys. Rev. B* **64**, 054514 (2001).
- [50] Michael Stone and Rahul Roy, "Edge modes, edge currents, and gauge invariance in p_x+ip_y superfluids and superconductors," *Phys. Rev. B* **69**, 184511 (2004).
- [51] J. A. Sauls, "Surface states, edge currents, and the angular momentum of chiral p-wave superfluids," *Phys. Rev. B* **84**, 214509 (2011).
- [52] S. Chatterjee, T. Wang, E. Berg, and M. Zaletel, to appear (2021).
- [53] Zhiyu Dong and Leonid Levitov, to appear (2021).

Supplementary material for:
“Unconventional superconductivity in systems with annular Fermi surfaces:
Application to rhombohedral trilayer graphene”

I. BAND STRUCTURE AND WAVE FUNCTIONS OF RHOMBOHEDRAL TRILAYER GRAPHENE

The band structure which is used to calculate superconducting pairing is based on 6×6 model [11, 12, 15]

$$h_{\mathbf{k}} = \begin{pmatrix} \delta + \Delta_1 + \Delta_2 & v_0\pi^* & v_4\pi^* & v_3\pi & 0 & \frac{\gamma_2}{2} \\ v_0\pi & \Delta_1 + \Delta_2 & \gamma_1 & v_4\pi^* & 0 & 0 \\ v_4\pi & \gamma_1 & -2\Delta_2 & v_0\pi^* & v_4\pi^* & v_3\pi \\ v_3\pi^* & v_4\pi & v_0\pi & -2\Delta_2 & \gamma_1 & v_4\pi^* \\ 0 & 0 & v_4\pi & \gamma_1 & -\Delta_1 + \Delta_2 & v_0\pi^* \\ \frac{\gamma_2}{2} & 0 & v_3\pi^* & v_4\pi & v_0\pi & \delta - \Delta_1 + \Delta_2 \end{pmatrix}, \quad (\text{S1})$$

where $\pi = \tau k_x + i k_y$ (τ is the valley index) and the Hamiltonian is written in the basis $(A_1, B_1, A_2, B_2, A_3, B_3)$ with A_i and B_i denoting different sublattice sites on layer i . Here the $v_i = \sqrt{3}a\gamma_i/2$, $a = 2.46\text{\AA}$ is the lattice constant of graphene, Δ_1 is proportional to the perpendicular electric field, and γ_i , δ , Δ_2 are the fixed material parameters: $\gamma_0 = 3.1\text{ eV}$, $\gamma_1 = 0.38\text{ eV}$, $\gamma_2 = -0.015\text{ eV}$, $\gamma_3 = -0.29\text{ eV}$, $\gamma_4 = -0.141\text{ eV}$, $\delta = -0.0105\text{ eV}$, $\Delta_2 = -0.0023\text{ eV}$ [15].

Fig. S1 shows the density of states (DOS) of the 6×6 model. Generally the system supports three types of Van Hove singularities (VHS): (1) disappearance of the central pocket for large (negative) hole densities, (2) transition from three pockets into six pockets (this regime is realized only for $\Delta_1 \gtrsim 18\text{ meV}$); and (3) merging of three or six pocket into annular or single contour. We note that at the displacement field $\Delta_1 \approx 18\text{ meV}$ where the phase with six pockets terminates, the dispersion features a higher order VHS. It is of the same type which was discussed recently for twisted bilayer graphene [37]. At the higher order VHS, the density of states diverges more strongly compared to a normal VHS. Annular FSs are present mostly for the hole densities and are responsible for the unconventional superconductivity discussed in the main text. In contrast, on the electron side, the annular Fermi surface is present for a very narrow range of chemical potentials ($\Delta\mu \leq 0.01\text{ meV}$ for $\Delta_1 \leq 20\text{ meV}$), it emerges once the three pockets merge at the VHS and rapidly disappears.

In addition to its complex Fermi surfaces, the 6×6 model differs from the simplified circularly symmetric model in that it incorporates the Bloch wave functions into the static polarization function and directly into the linearized gap equation. To understand the role of the wave functions in the calculations we show layer polarization and Berry curvature as a function of \mathbf{k} in Fig. S2. At low energies, the 6×6 model can be approximated by a 2×2 model, where only A_1 and B_3 sublattice sites contribute [12]. The layer polarization is defined as $(n_1 - n_3)/(n_1 + n_3)$, where $n_{1,3}$ are

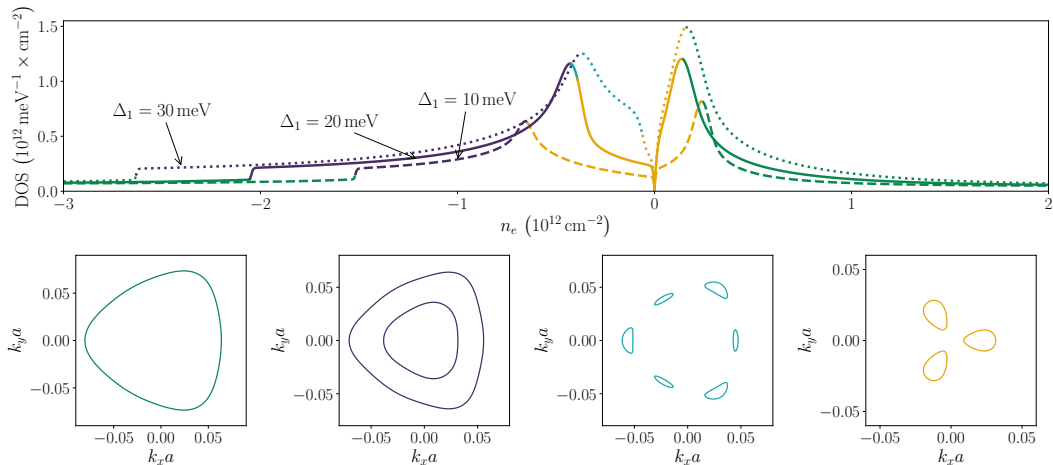


Figure S1. Density of states of 6×6 band model (S1) for three different values of the displacement field Δ_1 . Different regions of density corresponding to different FS topology are colored differently and representative FSs are shown in the lower panel. The FSs are for $\Delta_1 = 30\text{ meV}$ and $n_e = -2.63 \times 10^{12}\text{ cm}^{-2}$, $n_e = -1.35 \times 10^{12}\text{ cm}^{-2}$, $n_e = -0.13 \times 10^{12}\text{ cm}^{-2}$, $n_e = 0.14 \times 10^{12}\text{ cm}^{-2}$, respectively. The DOS data is generated at the temperature $T = 0.025\text{ meV}$ which regularizes VHSs.

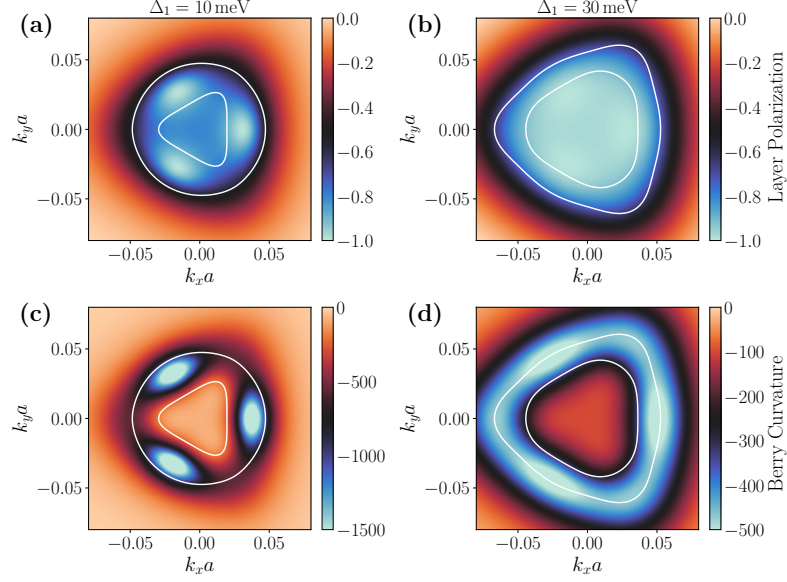


Figure S2. Evolution of layer polarization (a-b) and Berry curvature (c-d) with displacement field. The wave functions become more layer polarized upon increasing Δ_1 . First column shows layer polarization (a) and Berry curvature (c) for $\Delta_1 = 10$ meV; second column corresponds to $\Delta_1 = 30$ meV. While lines show FS corresponding to fixed density $n = -0.9 \cdot 10^{12} \text{ cm}^{-2}$ in both cases.

the densities in the first and third layers, respectively. While for densities corresponding to annular Fermi surfaces the wave function is strongly layer polarized, it still features three peaks both in polarization and Berry curvature figures. Increasing the displacement field Δ_1 enhances the layer polarization, thereby decreasing the influence of the wave function.

Finally, Fig. S3 shows the static polarization function $\Pi_{0,\mathbf{q}}$ close to the VHS point, both with and without taking into account the form factors $\Lambda_{\mathbf{k},\mathbf{q},\tau}$ due to the projection on a single band. The inclusion of the wave functions suppresses the additional peaks of the static polarization at finite \mathbf{q} . This results in an enhancement of effective interaction within RPA. While this by itself would increase the values of λ obtained in the calculation, one has to keep in mind that the wave functions also enter directly into the linearized gap equation [cf. Eq. (4) in the main text]. These two effects tend to cancel each other, making the combined effect from the inclusion of the wave functions not substantial for the amplitude of λ .

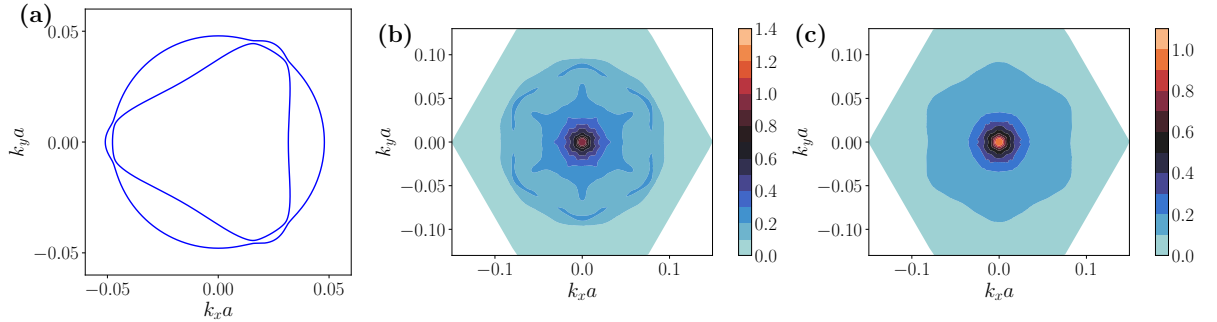


Figure S3. (a) Fermi surface of 6×6 band structure close to VHS. (b) Static polarization function $\Pi_{0,\mathbf{q}}$ without Bloch wave functions, and full polarization function (c) have similar structure. The $\Pi_{0,\mathbf{q}}$ is normalized by the density of states so that $\Pi_{0,0} = 1$. The additional peaks in (b) are not visible in (c), due to the structure of wave functions. The results are for $\Delta_1 = 20$ meV and $n_e = -0.42 \times 10^{12} \text{ cm}^{-2}$. Finite temperature $T = 0.015$ meV is used in polarization calculation to smoothen the singularities.

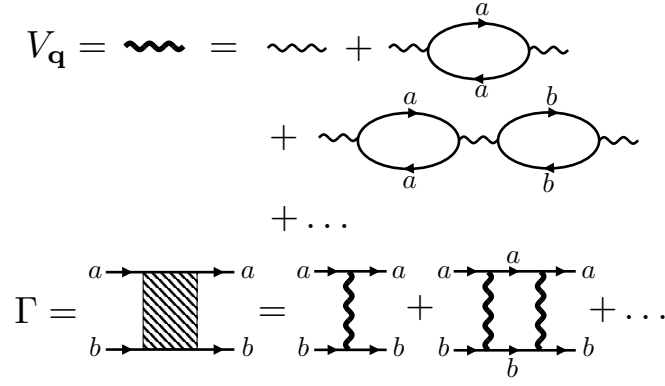


Figure S4. Diagrammatic representation of the effective interaction $V_{\mathbf{q}}$ and the pairing vertex Γ . Thin wiggly lines denote the Coulomb interaction, solid lines are fermionic propagators with flavor index a, b .

II. METHOD OF CALCULATING T_c

Here, we provide more details of our method of treating the superconductivity emergent from the Hamiltonian (1). To formally control the calculation, we imagine taking the limit of large number of electron flavors, $N \rightarrow \infty$ (with $N/2$ flavors in each of the two valleys). At the same time, we take the weak coupling limit such that $Ne^2/\epsilon \rightarrow \text{const.}$ To leading order in $1/N$, the effective interaction is then given by the RPA expression, Eq. (3) in the main text (see Fig. S4).

We can then use this interaction to calculate the pairing vertex Γ for inter-valley pairs (Fig. S4). Within our approach, the effective pairing interaction for a given flavor is of order $1/N$, which justifies the weak coupling treatment. Each additional term in the ladder summation is suppressed by $1/N$ but enhanced by a BCS logarithmic factor, of order $\log(W/T)$, and hence we need to sum the infinite ladder series, giving the usual BCS gap equation. Applying weak-coupling BCS theory is reasonable when making connection to experiments in RTG, since $T_c/E_F \sim 10^{-3}$ is much smaller than 1.

Note that our setup of the problem does not give the instabilities towards flavor symmetry breaking half and quarter metals seen in RTG; in the limit in which our calculations are justified, these effects are suppressed by factors of $1/N$. Treating superconductivity and flavor symmetry breaking on the same footing in a theoretically controlled way is difficult, and goes beyond our present analysis. On physical grounds, however, it is reasonable that upon changing the hole density towards the Van Hove point, superconductivity is first enhanced due to the increase in the density of states. By the Stoner criterion, the same increase in the density of states promotes flavor symmetry breaking transition that decreases the density of states, suppressing superconductivity. Hence, superconductivity and symmetry breaking appear close to each other in the phase diagram, even though they are not necessarily causally related.

Linearized gap equation

To derive Eq. (4) of the main text, we start from the standard BCS mean-field equation for the gap function:

$$\Delta_{\mathbf{k}} = - \int \frac{d^2 k'}{(2\pi)^2} V(\mathbf{k} - \mathbf{k}') |\Lambda_{\mathbf{k}, \mathbf{k}' - \mathbf{k}, +1}|^2 \frac{\tanh\left(\frac{E_{\mathbf{k}', 1}}{2T}\right)}{2E_{\mathbf{k}', 1}} \Delta_{\mathbf{k}'}, \quad (\text{S2})$$

where $E_{\mathbf{k}, \tau} = \sqrt{\varepsilon_{\mathbf{k}, \tau}^2 + |\Delta_{\mathbf{k}}|^2}$ is the dispersion of Bogoliubov quasi-particles. To get T_c , we keep only terms to linear order in $\Delta_{\mathbf{k}'}$ in the right hand side of (S2), replacing $E_{\mathbf{k}, 1}$ by $|\varepsilon_{\mathbf{k}, 1}|$. Furthermore, we linearize the dispersion near the FS, and change variables to Fermi surface coordinates such that $\int \frac{d^2 k'}{(2\pi)^2} = \int \frac{dk_{\parallel} dk_{\perp}}{(2\pi)^2}$, where k_{\parallel} and k_{\perp} are momenta parallel and perpendicular to the FS, and $\varepsilon_{\mathbf{k}, 1} \approx v_{\mathbf{k}} k_{\perp}$. Integrating over k_{\perp} gives a factor of $\frac{1}{v_{\mathbf{k}'}} \log(W/T)$, where W is an energy cutoff of the order of E_F . This gives Eq. (4).

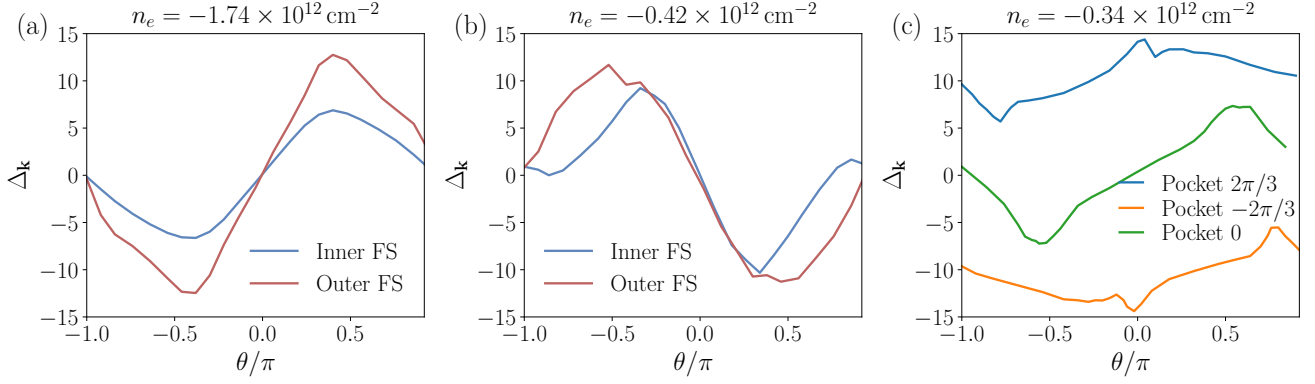


Figure S5. Angular dependence of the superconducting order parameter along the Fermi surface, for a p-wave state with a node along the x-axis (cf. Fig. 1 in the main text). (a) At large density, the inner pocket is small and the order parameter has a smaller amplitude there. (b) When the annulus is thin and both Fermi surfaces approach each other, the order parameters have comparable magnitude. (c) In the regime with three pockets, only the order parameter in the pocket along the nodal direction has a sign change, with the other two being of opposite sign with respect to each other. We note that the overall magnitude of the order parameter cannot be determined from the linearized gap equation and is fixed using normalization condition.

Solving linearized gap equation numerically

In this section we give the details of the numerical evaluation of λ and of the superconducting order parameter. To solve the linearized gap equation (4) numerically we first calculate the static polarization $\Pi_{0,\mathbf{q}}$ by taking a discrete square grid of momenta $k\mathbf{a}$ around the K and K' point in the range of $[-0.18, 0.18]$ with 2000 points in each direction. The static polarization is calculated at a finite temperature $T = 0.015$ meV to regularize the singularities of the polarization function. For each value of the density we choose angular equidistant points on the Fermi surface and calculate for those points the symmetric matrix

$$\widetilde{\mathcal{M}}_{\mathbf{k},\mathbf{k}'} = -\frac{1}{(2\pi)^2} \sqrt{\frac{\Delta k \Delta k'}{v_{\mathbf{k}} v_{\mathbf{k}'}}} V_{\mathbf{k}-\mathbf{k}'} |\langle u_{\mathbf{k},+1} | u_{\mathbf{k}',+1} \rangle|^2, \quad (\text{S3})$$

which is the discretized version of the linear operator defined in the main text. Δk is the distance between two points on the Fermi surface. The number of points on the Fermi surface is chosen such that Δk is approximately 0.25 of the mean radius of the pocket but not smaller than 5 discrete grid points to regularize the divergence of λ when density of states diverges. The largest eigenvalue of $\widetilde{\mathcal{M}}_{\mathbf{k},\mathbf{k}'}$ corresponds to λ presented in the main text. The superconducting order parameter is given by $\Delta_{\mathbf{k}} = \phi_{\mathbf{k}} \sqrt{v_{\mathbf{k}} / \Delta k}$, where $\phi_{\mathbf{k}}$ is the eigenvector of $\widetilde{\mathcal{M}}_{\mathbf{k},\mathbf{k}'}$, i.e. it fulfills $\widetilde{\mathcal{M}}_{\mathbf{k},\mathbf{k}'} \phi_{\mathbf{k}'} = \lambda \phi_{\mathbf{k}}$. Some examples for the superconducting order parameter calculated this way are shown in Fig. S5.

Superconductivity in the conduction band

We comment briefly on superconductivity on the electron side, where an annular Fermi surface is not realized for the system parameters of RTG. Fig. S6 shows the dependence of the coupling constant λ on the electron density for different values of the displacement field Δ_1 . While a p-wave superconducting instability is realized for this case as well, the presence of only a single Fermi pocket after the three small pockets have merged results in a more rapid decrease of λ with increasing electron density. This naturally leads to smaller superconducting regions or absence of thereof, consistent with experimental data [16]. Near VHS a Stoner transition occurs, effectively making the region with a large density of states inaccessible. Thus, the more rapid decrease of λ away from VHS observed for the conduction band gives rise to a smaller range of densities where T_c is within reach of experimentally achievable temperatures.

III. SUSCEPTIBILITY AND PAIRING IN THE CIRCULARLY SYMMETRIC MODEL

In the following, we consider the more convenient parametrization of the “Mexican hat dispersion”, $\epsilon_{\mathbf{k}} = \varepsilon_0((k^2 - k_0^2)^2 - \bar{\mu})/k_0^4$. This differs from the one used in the main text by an overall minus sign, and uses different units for

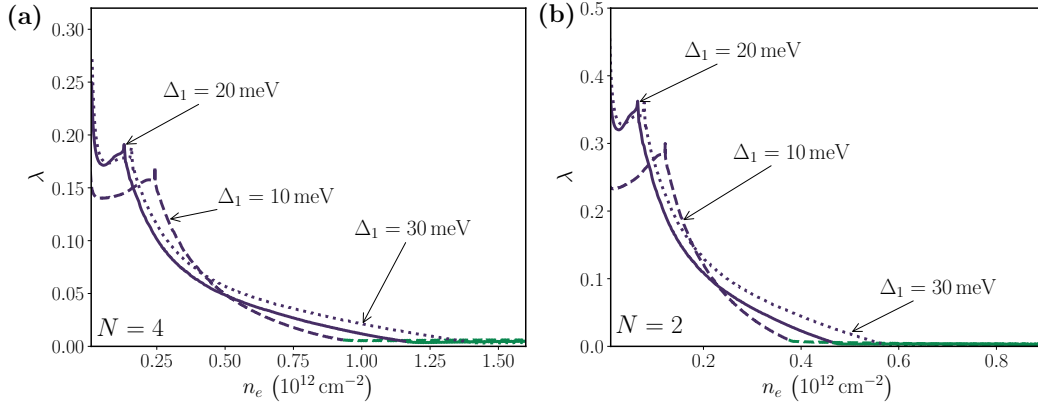


Figure S6. Coupling constant λ as a function of electron density for different values of the displacement field Δ_1 projected into the lowest electron band. (a) for the unpolarized $N = 4$ state and (b) for the polarized $N = 2$ state. In the broad range of densities the emergent SC order parameter is p-wave like (purple), while at larger densities it has 8 nodes and resembles g-wave (green). Since both p- and g-wave belong to the same representation of C_{3v} , the change in the nature of the order parameter happens via an avoided crossing of the largest eigenvalues.

the chemical potential $\bar{\mu} = -k_0^4 \mu / \varepsilon_0$. This choice of units highlights the two natural parameters that are present for this dispersion, the overall scale ε_0 , and the size of the annulus as given by k_0 . The locations of the FSs are given by $k_{F1}^2 = k_0^2 + \sqrt{\bar{\mu}}$ and $k_{F2}^2 = k_0^2 - \sqrt{\bar{\mu}}$, the total number density is $n = N\sqrt{\bar{\mu}}/2\pi$. We will further use the abbreviation $q' = \sqrt{4k_0^2 - q^2}$. At $T = 0$, the susceptibility can be written as

$$\Pi_{0,q} = N \int \frac{d^2 k}{4\pi^2} \frac{\Theta(-\varepsilon_{\mathbf{k}}) - \Theta(-\varepsilon_{\mathbf{k}+\mathbf{q}})}{\varepsilon_{\mathbf{k}+\mathbf{q}} - \varepsilon_{\mathbf{k}}} = \frac{N}{4\pi^2} \int_{k_{F2}}^{k_{F1}} k dk \int_{-\pi}^{\pi} d\theta \left(\frac{1}{\varepsilon_{\mathbf{k}+\mathbf{q}} - \varepsilon_{\mathbf{k}}} - \frac{1}{\varepsilon_{\mathbf{k}} - \varepsilon_{\mathbf{k}-\mathbf{q}}} \right). \quad (\text{S4})$$

The angular integral is relatively straightforward, but as usual requires some care with regards to branch cuts in logarithmic functions. A bit more subtle is that a δ -function appears in the radial dependence, a fact which is confirmed by a numerical integration of the regulated expression. After angular integration we obtain the following expression:

$$\Pi_{0,q} = \frac{N}{4\pi^2} \frac{k_0^4}{\varepsilon_0} \int_{k_{F2}}^{k_{F1}} \frac{4k dk}{q(k^2 - k_0^2)} \text{Re} \left[\frac{i\pi q \text{sgn}(4k_0^2 - 2q^2 - 4k^2)}{2 \sqrt{8k_0^2 k^2 - 4k^4 - q'^4}} \right. \\ \left. - \frac{\text{arctanh} \frac{q+2k}{\sqrt{4k^2 - q^2}} + \text{arctanh} \frac{q-2k}{\sqrt{4k^2 - q^2}}}{\sqrt{4k^2 - q^2}} + \frac{\pi^2(k^2 - k_0^2)}{4\sqrt{4k^2 - q^2}} \delta(k - k_0) \right]. \quad (\text{S5})$$

This is simple enough to perform the radial integration. Surprisingly, the contribution from the δ -function allows to combine the logarithms from the lower and upper boundary into one expression by canceling the additional contribution that is left from switching between branch cuts. This greatly simplifies the final result into

$$\Pi_{0,q} = -\frac{N}{4\pi^2} \frac{k_0^4}{\varepsilon_0} \text{Re} \left[\frac{2\pi}{qq'} \arctan \frac{\sqrt{4\bar{\mu} - 2k_0^2 q^2 + q^4}}{qq'} \Theta(k_{F1} - k_{F2} - q) + \frac{i\pi}{qq'} \log \frac{2\sqrt{\bar{\mu}} + q'^2 + q' \sqrt{q'^2 + 4\sqrt{\bar{\mu}}}}{2\sqrt{\bar{\mu}} - q'^2 - q' \sqrt{q'^2 - 4\sqrt{\bar{\mu}}}} \right]. \quad (\text{S6})$$

For completeness, we also present the susceptibility for $\bar{\mu} > k_0^4$ (i.e. a single large Fermi circle after the annulus closes in the middle) which coincides with the solution for a dispersion where $k_0^2 < 0$ (i.e. a single large Fermi circle due to a positive mixed term in the dispersion). In these latter cases, it is

$$\Pi_{0,q} = -\frac{N}{4\pi^2} \frac{k_0^4}{\varepsilon_0} \text{Re} \left[\frac{\pi}{qq'} \arctan \frac{\sqrt{4\bar{\mu} - q^2 q'^2}}{qq'} + \frac{\pi}{qq'} \arctan \frac{2k_0^2 - q^2}{qq'} + \frac{i\pi}{qq'} \log \frac{k_0^2(q'^2 + 2\sqrt{\bar{\mu}} + q' \sqrt{q'^2 + 4\sqrt{\bar{\mu}}})}{\sqrt{\bar{\mu}}(q^2 - 2k_0^2 - iqq')} \right], \quad (\text{S7})$$

where, as mentioned k_0^2 can assume values smaller than zero.

We can use expression Eq. (S6) to obtain some analytical insight regarding the effective interaction V_q and the parameter λ . In the limit of a thin ring, we can drop the weak correction at small q and evaluate the logarithm to

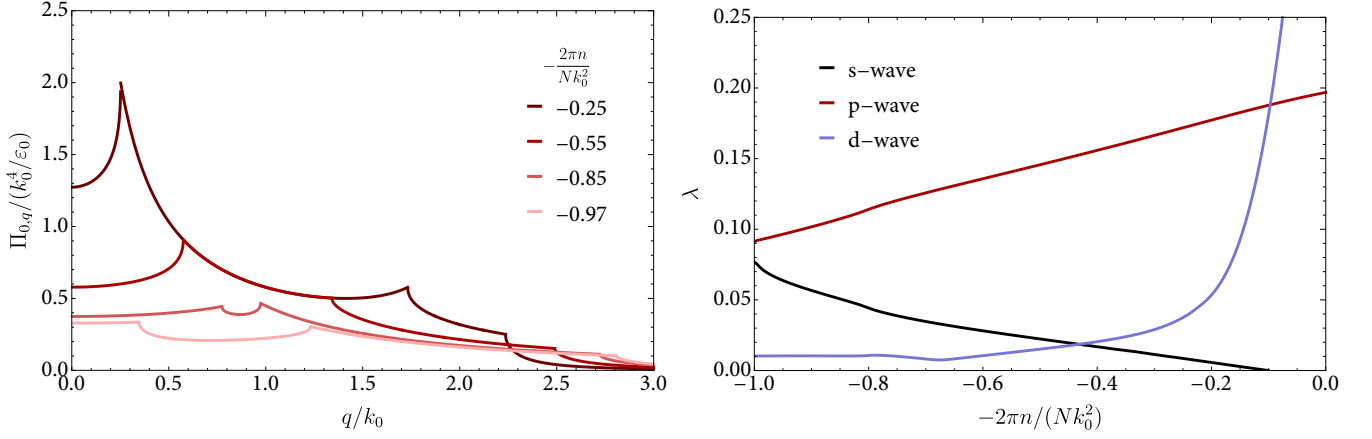


Figure S7. Mexican hat dispersion. (a) Dimensionless particle-hole susceptibility $\Pi_{0,q}$ as a function of the normalized momentum transfer q/k_0 . (b) Strong interaction limit $V_q = \Pi_{0,q}^{-1}$. Shown are the absolute value of the most negative eigenvalues in the s,p,d angular momentum channels as a function of normalized density. Both figures are for a number of flavors $N = 4$, the total number density is n .

obtain

$$\Pi_{0,q} = \frac{N}{4\pi^2} \frac{k_0^4}{\varepsilon_0} \text{Re} \left[-\frac{i\pi}{qq'} (-i\pi) \right] \quad (\text{S8})$$

The susceptibility then diverges around $q = 0$, so that one can safely take the strong interaction limit, yielding

$$V_q = \frac{4}{N} \frac{k_0^4}{\varepsilon_0} \text{Re} [qq']. \quad (\text{S9})$$

For $n \rightarrow 0$ (i.e. $\bar{\mu} \rightarrow 0$), the momentum transfer becomes approximately $qq' = k_0^2 |\sin \theta|$. Inserting these simplifications into the linearized gap equation yields for the d-wave channel the matrix elements

$$\mathcal{M}_{11} = \mathcal{M}_{22} = \mathcal{M}_{12} = \frac{k_0^2}{3\pi^3 n}. \quad (\text{S10})$$

The matrix then has the largest eigenvalue $\lambda = 2\mathcal{M}_{22}$, which diverges like n^{-1} . In the vicinity of $\bar{\mu} \rightarrow k_0^4$, in the p-wave channel λ can also be recovered analytically. We approximate the susceptibility as

$$\Pi_{0,q} = \frac{N}{4\pi^2} \frac{k_0^4}{\varepsilon_0} \text{Re} \left[\frac{-i\pi}{qq'} \log \frac{q^2 - 6k_0^2 - q'\sqrt{8k_0^2 - q^2}}{2k_0^2 - q^2 + iqq'} \right]. \quad (\text{S11})$$

Inserting the limiting values for $k_{F2} = 0$ and $k_{F1} = 2k_0$ results in $\Pi_{11}^{-1} = 0$ and

$$\frac{N}{4\pi^2} \frac{k_0^4}{\varepsilon_0} \Pi_{12}^{-1} = \frac{4k_0^2}{\pi^2} \quad (\text{S12})$$

$$\frac{N}{4\pi^2} \frac{k_0^4}{\varepsilon_0} \Pi_{22}^{-1} = \frac{4k_0^2}{\pi} \text{Im} \left[\frac{\log(\alpha_+(\theta)\alpha_-(\theta))}{\sqrt{2\cos\theta} |\sin \frac{\theta}{2}|} \right]^{-1}, \quad (\text{S13})$$

where $\alpha_{\pm}(\theta) = (1 \pm 2\cos\theta + 2\sqrt{\cos\theta \pm 1}\sqrt{\cos\theta})$. The last expression is captured reasonably well by $\sim -4\sqrt{2}k_0^2 |\sin \frac{\theta}{2}| / (\pi \log(3 - 2\sqrt{2}))$, but we will forego this simplification. Integration in the p-wave channel using Eq. (S13) results in the matrix elements $\mathcal{M}_{11} = \mathcal{M}_{12} = 0$ and $\mathcal{M}_{22} = 0.37/N$. The largest eigenvalue is therefore $\lambda = \mathcal{M}_{22}$, in excellent agreement with a numerical evaluation.

We note that the solution for a radial dispersion with $k_0^2 < 0$ [Eq. (S7)], which is a radially symmetric dispersion more representative of the electron side, results in really small values for $\lambda < 0.01$, far below the ones found using the tight-binding dispersion (Fig. S6). We thus conclude that the latter finding is a parametric effect which depends strongly on the amount of trigonal warping in the system and on the proximity to the VHS.

IV. SELECTION OF CHIRAL SUPERCONDUCTIVITY BELOW T_c

In this Section, we discuss the nature of the p-wave superconducting state. At T_c , there are two degenerate components of the order parameter, which we denote by Δ_x and Δ_y . Below T_c , these components can either combine into a chiral $\Delta_x + i\Delta_y$ state that breaks time reversal symmetry, or into a nematic superconducting $\alpha\Delta_x + \beta\Delta_y$ state (where α and β are real), breaking C_3 rotational symmetry. To determine which state is preferred, we need to solve the nonlinear BCS gap equation and compare their condensation energies. Near T_c , this can be done by considering the quartic terms in the Landau free energy functional. Up to fourth order in $\Delta_{x,y}$, the most general free energy density compatible with C_3 and time reversal symmetries can be written as

$$f = r(T) (|\Delta_x|^2 + |\Delta_y|^2) + \frac{u}{2} (|\Delta_x|^2 + |\Delta_y|^2)^2 + \frac{u_1}{2} (\Delta_x^* \Delta_y - \Delta_y^* \Delta_x)^2 \quad (\text{S14})$$

where, as usual, $r(T) \propto (T - T_c)/T_c$, and stability requires that $u > 0$ $u_1 > -u$. $u_1 > 0$ ($u_1 < 0$) favors chiral (nematic) SC, respectively.

Within BCS theory, the quartic terms are determined by the non-interacting band structure. The sign of u_1 can be determined by expanding the second term in Eq. (S14) and examining the $(\Delta_x^*)^2 \Delta_y^2$ contribution. This contribution comes from the diagram shown in Fig. S8. Denoting the solutions of the linearized gap equation [Eq. (4) in the main text] as $\Delta_{a,\mathbf{k}} = \Delta_a f_a(\mathbf{k})$ with $a = x, y$ and $f_{x,y}(\mathbf{k})$ are real functions (such a choice is possible due to time reversal symmetry), we can express u_1 as

$$u_1 = \frac{1}{2} T \sum_{\omega_n} \int \frac{d^2 k}{(2\pi)^2} \frac{f_x^2(\mathbf{k}) f_y^2(\mathbf{k})}{(\omega_n^2 + \varepsilon_{\mathbf{k},+}^2)^2} > 0. \quad (\text{S15})$$

Here, $\omega_n = \pi(2n+1)T$ are Matsubara frequencies. Hence, within our model, the chiral SC is favored below T_c . Note that this conclusion relies only on the C_3 symmetry, and does not depend on any microscopic details of the system.

V. ROLE OF HUND'S COUPLING

The Hund's term lifts the degeneracy between the singlet and triplet SC states. We assume the following simple form for H_{Hund} :

$$H_{\text{Hund}} = - \int d^2 r \int d^2 r' J_H(\mathbf{r} - \mathbf{r}') \mathbf{S}_+(\mathbf{r}) \cdot \mathbf{S}_-(\mathbf{r}'). \quad (\text{S16})$$

Here, $\mathbf{S}_\tau(\mathbf{r})$ is the spin density in valley τ ,

$$S_\tau^j(\mathbf{r}) = \frac{1}{2} \sum_{\ell, \sigma} \sum_{\alpha, \beta=\uparrow, \downarrow} \psi_{\ell, \sigma, \tau, \alpha}^\dagger(\mathbf{r}) s_{\alpha\beta}^j \psi_{\ell, \sigma, \tau, \beta}(\mathbf{r}), \quad (\text{S17})$$

where $j = x, y, z$ and s^j are Pauli matrices in spin space. $J_H(\mathbf{r})$ decays rapidly in real space. Naively, its typical range is the lattice spacing a , since microscopically, the Hund's coupling originates from lattice-scale interactions. As mentioned in the main text, J_H receives contributions from both Coulomb and electron-phonon interactions, and may have either sign.

Projecting H_{Hund} to the valence band, it is useful to rewrite it in the Cooper channel as

$$H_{\text{Hund}} = - \frac{1}{8L^2} \sum_{\mathbf{k}, \mathbf{k}', \mathbf{q}} \tilde{J}_H(\mathbf{k} - \mathbf{k}') \Lambda_{\mathbf{k}', \mathbf{k}, +1} \Lambda_{-\mathbf{k}'+\mathbf{q}, -\mathbf{k}+\mathbf{q}, -1} [3\Phi_t^\dagger(\mathbf{k}', \mathbf{q}) \cdot \Phi_t(\mathbf{k}, \mathbf{q}) - \Phi_s^\dagger(\mathbf{k}', \mathbf{q}) \Phi_s(\mathbf{k}, \mathbf{q})], \quad (\text{S18})$$

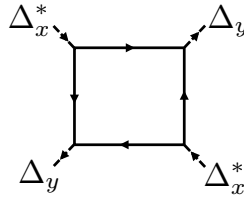


Figure S8. Diagram for the calculation of the quartic term u_1 in Eq. (S14).

where $\tilde{J}_H(\mathbf{q}) = \int d^2r e^{-i\mathbf{q}\cdot\mathbf{r}} J_H(\mathbf{r})$, and

$$\begin{aligned}\Phi_t(\mathbf{k}, \mathbf{q}) &= c_{-\mathbf{k}+\mathbf{q},-}^T (is_y \mathbf{s}) c_{\mathbf{k},+}, \\ \Phi_s(\mathbf{k}, \mathbf{q}) &= c_{-\mathbf{k}+\mathbf{q},-}^T (is_y) c_{\mathbf{k},+}.\end{aligned}\tag{S19}$$

Here, $c_{\mathbf{k},\tau}^T = (c_{\mathbf{k},\tau,\uparrow}, c_{\mathbf{k},\tau,\downarrow})$, and Φ_s, Φ_t are the singlet and triplet pairing operators, respectively.

The Hund's term is incorporated in the linearized gap equation [(4)] by adding to the linear operator \mathcal{M} a term \mathcal{M}_H defined by its action on the singlet and triplet gap functions, $(\Delta_s)_{\mathbf{k}}$ and $(\Delta_t)_{\mathbf{k}}$ respectively, as

$$\begin{aligned}(\mathcal{M}_H \Delta_s)_{\mathbf{k}} &= -\frac{1}{8} \int \frac{dk_{\parallel}'}{(2\pi)^2 v_{\mathbf{k}'}} \tilde{J}_H(\mathbf{k} - \mathbf{k}') |\Lambda_{\mathbf{k},\mathbf{k}-\mathbf{k}',+1}|^2 (\Delta_s)_{\mathbf{k}'}, \\ (\mathcal{M}_H \Delta_t)_{\mathbf{k}} &= \frac{3}{8} \int \frac{dk_{\parallel}'}{(2\pi)^2 v_{\mathbf{k}'}} \tilde{J}_H(\mathbf{k} - \mathbf{k}') |\Lambda_{\mathbf{k},\mathbf{k}-\mathbf{k}',+1}|^2 (\Delta_t)_{\mathbf{k}'}.\end{aligned}\tag{S20}$$

The dimensionless SC coupling constants for singlet and triplet pairing, $\lambda_{s,t}$, satisfy $(\mathcal{M} + \mathcal{M}_H) \Delta_{s,t} = \lambda_{s,t} \Delta_{s,t}$.

To zeroth order in \tilde{J}_H , the singlet and triplet channels are degenerate. Denoting the solution of the linearized gap equation in this case by $\Delta_{\mathbf{k}}$, we can estimate the singlet-triplet splitting $\Delta\lambda_{st} \equiv \lambda_s - \lambda_t$ using first-order perturbation theory as

$$\Delta\lambda_{st} \approx -\frac{1}{2} \frac{\int_{k_{\parallel}} \int_{k_{\parallel}'} \Delta_{\mathbf{k}}^* \tilde{J}_H(\mathbf{k} - \mathbf{k}') |\Lambda_{\mathbf{k},\mathbf{k}-\mathbf{k}',+1}|^2 \Delta_{\mathbf{k}'}}{\int_{k_{\parallel}} |\Delta_{\mathbf{k}}|^2},\tag{S21}$$

where we introduced the shorthand notation $\int_{k_{\parallel}} \equiv \int \frac{dk_{\parallel}}{(2\pi)^2 v_{\mathbf{k}}}$. First, let us neglect the momentum dependence of $\tilde{J}_H(\mathbf{q})$ (i.e., we assume that the Hund's term is local in real space). Then, denoting $\tilde{J}_H(\mathbf{q}) = J_{H,0}$, we find that $J_{H,0} > 0$ always favors triplet pairing ($\Delta\lambda_{st} \leq 0$), as expected for a ferromagnetic Hund's coupling.

However, if $\Delta_{\mathbf{k}}$ has p-wave symmetry, then for a momentum-independent \tilde{J}_H we get $\Delta\lambda_{st} = 0$. This is since in this case, $\Delta_{\mathbf{k}}$ is annihilated by \mathcal{M}_H . This can be checked directly using Eq. (S20), using the symmetry properties of the system under C_3 . Lifting the singlet-triplet degeneracy requires \tilde{J}_H to be momentum dependent. In order to understand how the momentum dependence of \tilde{J}_H gives rise to a singlet-triplet splitting in the p-wave case, we expand $\tilde{J}_H(\mathbf{q})$ around $\mathbf{q} = 0$, writing it is as

$$\tilde{J}_H(\mathbf{q}) = J_{H,0} + J_{H,2}(qa)^2 + O(q^4).\tag{S22}$$

Note that no other terms are allowed by the C_3 symmetry to second order in \mathbf{q} . Assuming that $\Delta_{\mathbf{k}}$ has angular momentum $m = 1$, i.e. $\Delta_{R_3\mathbf{k}} = e^{2i\pi/3} \Delta_{\mathbf{k}}$ where R_3 is a rotation matrix by $2\pi/3$, we can rewrite Eq. (S21) as

$$\Delta\lambda_{st} \approx \frac{J_{H,2} a^2}{4} \frac{\int_{k_{\parallel}} \int_{k_{\parallel}'} |\Lambda_{\mathbf{k},\mathbf{k}-\mathbf{k}',+1}|^2 \Delta_{\mathbf{k}}^* (k_x + ik_y) (k'_x - ik'_y) \Delta_{\mathbf{k}'}}{\int_{k_{\parallel}} |\Delta_{\mathbf{k}}|^2}.\tag{S23}$$

The integral in the numerator of Eq. (S23) is non-negative and is not required to vanish by symmetry. Therefore, in the p-wave phase, $J_{H,2} > 0$ ($J_{H,2} < 0$) favors singlet (triplet) pairing, respectively.

In order to demonstrate the effects of $J_{H,0}$ and $J_{H,2}$ on the singlet-triplet splitting, we show $\Delta\lambda_{st}$ as a function of density in the rotationally-symmetric model for both the p-wave and extended s-wave phases in Fig. S9. The coefficients of the correction terms are universal in that they do not depend on the flavor number N . For extended s-wave, the main correction comes from the momentum independent part $J_{H,0}$, which nearly cancels due to the sign change of the order parameter between both Fermi surfaces, leaving only a small magnitude $< 0.01 k_0^2 J_{H,0}/\varepsilon_0$ (Fig. S9). In the case of p-wave order the part from $J_{H,0}$ is identically zero. To determine the next contribution at order q^2 , we use that for p-wave and for a thin ring it holds approximately that $\mathcal{M}_{11} = \mathcal{M}_{12} = \mathcal{M}_{22}$, making the first perturbation in $J_{H,2}$ independent of the value of \mathcal{M} . The result is then $\Delta\lambda = \frac{\varepsilon_0}{8\pi\sqrt{\mu}} J_{H,2} (ak_0)^2$, which diverges upon taking the limit $n \rightarrow 0$ ($\sqrt{\mu} \rightarrow 0$). Note that the correction to the d-wave channel vanishes identically both for $J_{H,0}$ and $J_{H,2}$. As mentioned before, in the singlet pairing channel the correction due to the Hund's coupling is further multiplied by $-1/4$, while the factor is $+3/4$ for the triplet channel.

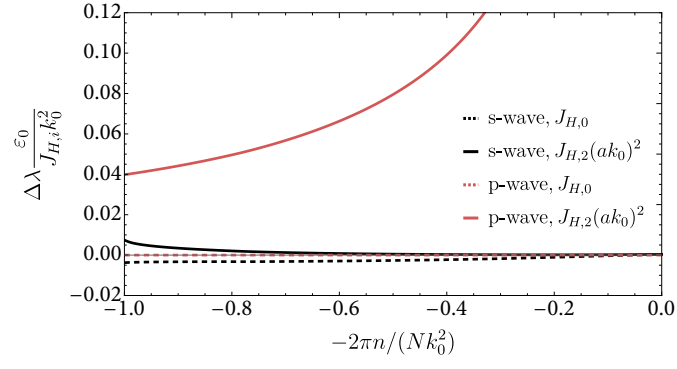


Figure S9. Effect of the Hund's coupling on λ for a circularly symmetric dispersion. For small J_H , the normalized correction $\Delta\lambda$ is proportional to J_H , namely $\Delta\lambda \propto J_{H,0}$ for s-wave order and $\Delta\lambda \propto J_{H,2}(ak_0)^2$ for p-wave order. As shown in the text, in the case of p-wave, the correction has a divergent coefficient in the limit $n \rightarrow 0$. Note that $J_{H,i}$ is normalized in units of density of states k_0^2/ε_0 . Furthermore, there is a multiplicative factor for the spin configuration depending whether the pairing is in the singlet or triplet channel.